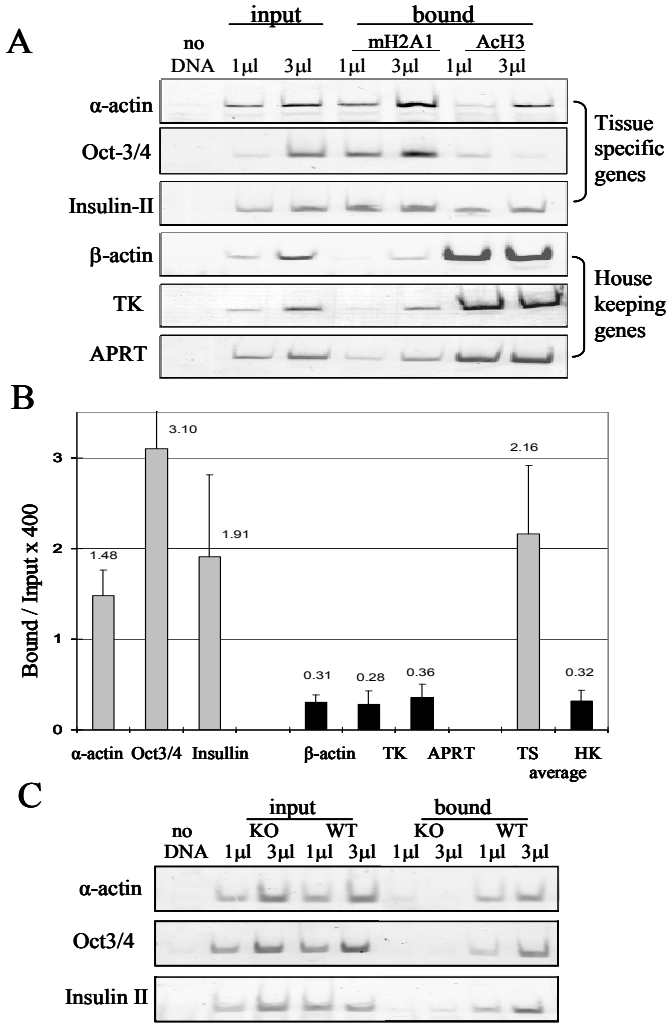

Supplementary Figure 1: **Validation of MacroH2A1 specific chromatin immunoprecipitation.**

A: Chromatin immunoprecipitation on mouse embryonic fibroblasts (MEFs) chromatin using anti-macroH2A1 and anti-acetylated H3 (as a marker for active chromatin). Input and bound fractions were analyzed by semi-quantaitive PCR. MacroH2A1 is enriched in non-expressed tissue-specific genes compared to house keeping genes while Acetylated-H3 shows the inverse pattern.

B: MacroH2A1 bound and input signals shown in **A** were quantified using Image Gauge software. The values of bound / input are shown for each gene and the average value for TS – tissue specific genes and HK – house keeping genes.

C: Chromatin immunoprecipitation on mouse ES cells (mES) using anti-macroH2A1 antibody. The absence of signal from the bound fraction of macroH2A1 deficient cells (KO) confirms the specificity of the antibody and ChIP procedure.

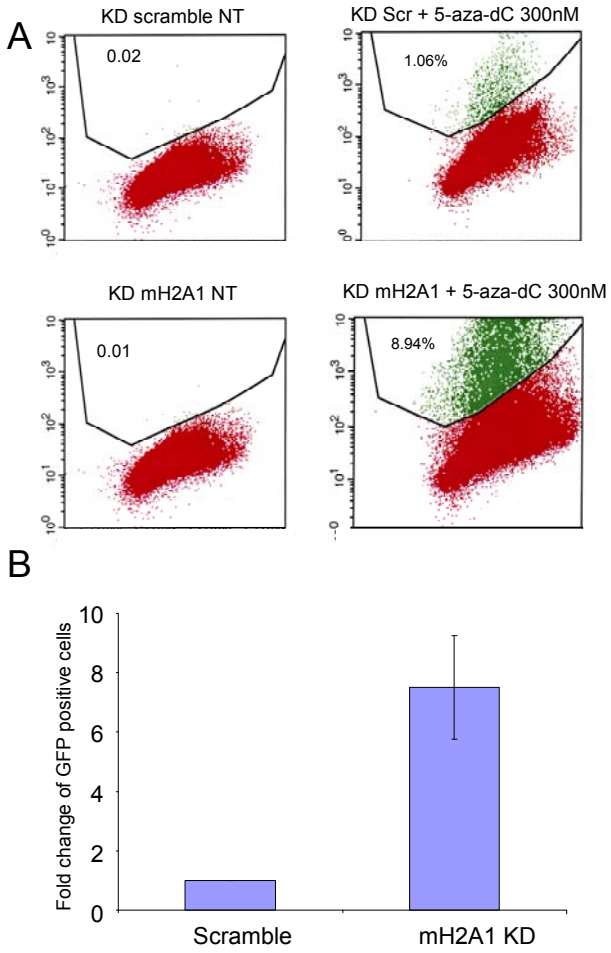

Supplementary Figure 2: reactivation of GFP reporter from the inactive X following mH2A1 KD.

A: Mouse fibroblasts with non-random x-inactivation and a silenced GFP repor"ter on their inactive X (1) were infected with mH2A1 shRNA or scrambled sequence shRNA. The effect of macroH2A1 knockdown and 5-aza-dC (300nM) for 3 days on expression of GFP was analyzed using FACS. In agreement with Hernandez-Munoz et al.(2), following DNA demethylation, higher degree of reactivation was observed in macroH2A1 deficient cells compared to controls. Plots show percent of GFP positive cells of all live cells.

B: Similar results as A were observed in 4 additional repeated experiments and the average (+/- SD) fold increase in GFP positive cells is shown in the graph.

TIMP3

Cells	nM aza	Methyled CpG
SW480	-	2%
RKO	500nM	43%
RKO	200nM	69%
RKO	50nM	77%
RKO	-	86%

MLH1

Cells	nM aza	Methyled CpG
SW480	-	0%
RKO	500nM	56%
RKO	200nM	83%
RKO	50nM	95%
RKO	-	97%

p16

Cells	nM aza	Methyled CpG
SW480	-	95%
RKO	500nM	70%
RKO	200nM	81%
RKO	50nM	91%
RKO	-	100%

Supplementary Figure 3: Dose dependant DNA demethylation of CpG island of silenced TSGs after 5-aza-dC treatment.

RKO cells were treated with increasing concentrations of 5-aza-dC for 6 days (DNA was collected from RKO samples presented in figure 5). DNA treated with Sodium bisulfite (Zymo Research), PCR amplified with locus specific bisulfite universal primers, cloned into T-vector (Promega) and sequenced.

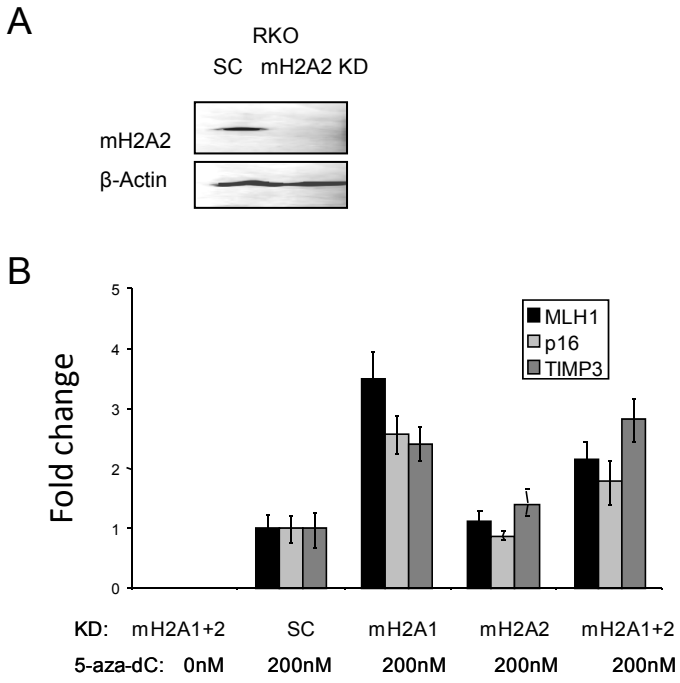

Supplementary Figure 4: KD of macroH2A2 in RKO cells does not promote further reactivation of silenced genes.

A: Western blot showing levels of macroH2A2 in RKO cells infected with Lentiviral macroH2A2 specific shRNA or scrambled shRNA.

B: Real-time RT-PCR analysis of MLH1, p16 and TIMP3 expression in RKO cells with macroH2A1 and/or macroH2A2 knockdown following treatment with 5-aza-dC. Graph shows fold change in expression level relative to control (scrambled KD) treated with 200nM 5-aza-dC.

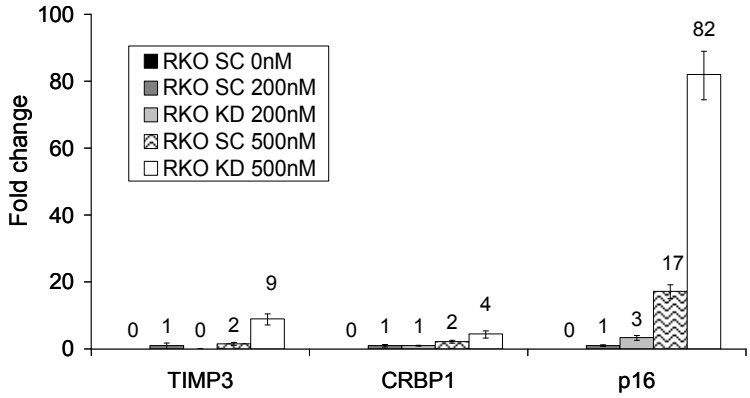

Supplementary Figure 5: reactivation of TSGs in cells subject to ChIP

RNA samples corresponding to samples analyzed by ChIP in figure 5 were analyzed for reactivation of silenced genes. Real-time RT-PCR analysis of TIMP3, CRBP1 and p16 expression in RKO transduced with scramble or macroH2A1 KD following increase dosage of 5-aza-dC. Graph shows fold change in expression level relative to control (scrambled KD) treated with 200nM 5-aza-dC.

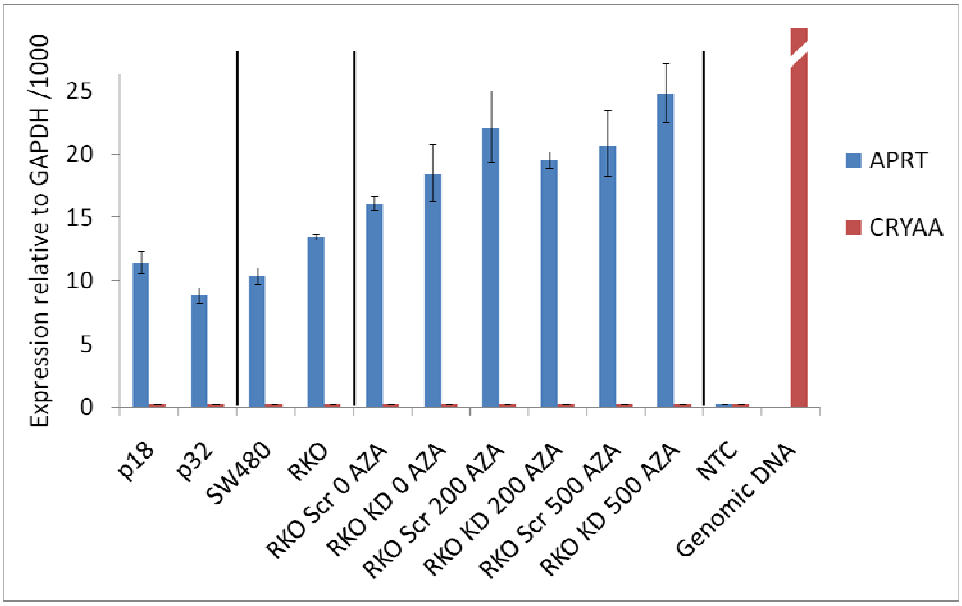

Supplementary Figure 6: Expression of APRT and CRYAA in samples subject to ChIP: The APRT locus is transcriptionally active in all samples while the CRYAA locus is repressed. Genomic DNA was used as positive control for CRYAA PCR

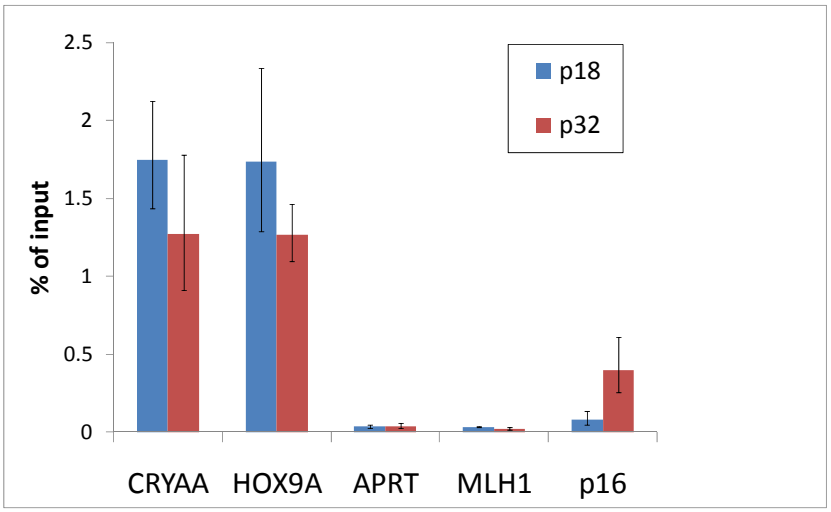

Supplementary Figure 7: MacroH2A1 ChIP results from Figure 1 presented as % of input (without normalization to the positive control CRYAA)

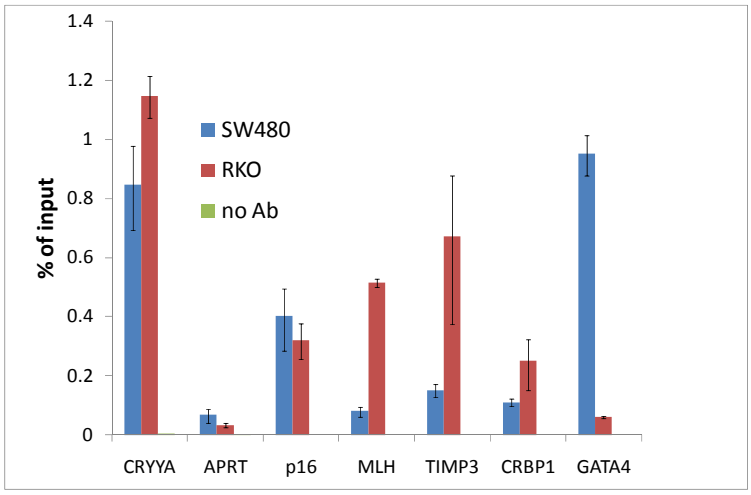

Supplementary Figure 8: MacroH2A1 ChIP results from Figure 2 presented as % of input (without normalization to the positive control CRYAA)

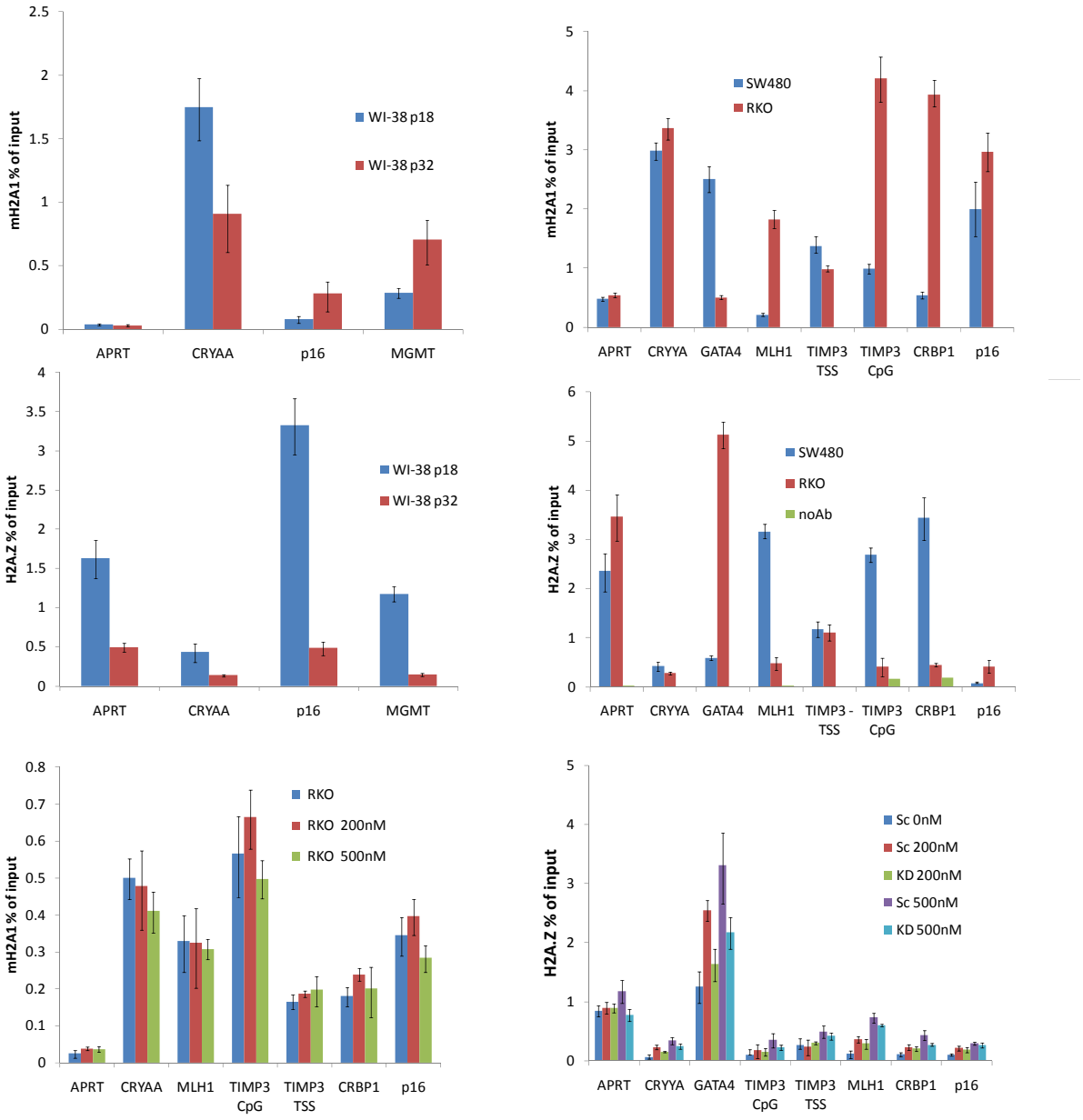

Supplementary Figure 9: ChIP results from Figure 1 presented as % of input (without normalization to the positive control: CRYAA for macroH2A1 and APRT for H2A.Z)

Supplementary methods:

Bioinformatic analysis: MacroH2A1 chip-chip data from IMR90 lung fibroblasts (GEO accession GSE18633) was correlated with data on aberrant methylation in WI-38 lung fibroblasts obtained on Illumina Humanmethylation27 bead arrays. Aberrant methylation was defined as low methylation value (beta<0.25) in primary WI-38 cells and high methylation value (beta>0.7) in late passage cells.

For each probe on the Illumina array, a MacroH2A1 enrichment score was assigned by averaging the macroH2A1 values of all the Chip probes located within the region (-300bp to +300 bp) relative to Illumina probe.

For figure 6A we restricted the analysis to 18,976 sites located within CpG islands (and excluding probes from Chromosome X, since WI-38 cells are female). Sites were grouped into 25 equal size groups according to macroH2A1 enrichment value, from the least enriched sites (group 1) to the most enriched (group 25). For each group we determined the number of de-novo DNA methylation events in late passage WI-38 cells compared to primary WI-38.

Genomewide Chip-Seq data on H3K27me3 in human lung fibroblasts generated as part of the Broad Institute Epigenomics initiative was downloaded from UCSC genome browser http://genome.ucsc.edu/cgi-bin/hgTrackUi?hgsid=169874931&c=chr21&g=wgEncodeBroadChipSeq

H3K27me3 levels at CpG sites analyzed on Illumina array (Repersenting a genomic region of 300bp was extracted.

For figure 6B 18,976 (as above) were grouped into 36 groups according to macroH2A1 and K3K27 enrichment values, from the least enriched sites (group 1) to the most enriched (group 6) in each dimention. For each group we determined the percentage of de-novo DNA methylation events in late passage WI-38 cells compared to primary WI-38.

Table 1: primers used in this work

Primer name	Forward	Reverse	Position relative to TSS	Ref.
APRT ChIP	GCCTTGACTCGCACTTTTGT	TAGGCGCCATCGATTTTAAG	-117 -201	(3)
APRT RT	ACTCTGTGGGCCTCCTATTCC	TTCTGAATCTCCAGCTCAGCCT		
CDKN2A ChIP5	AGCACTCGCTCACAGCGTC	CTGTCCCTCAAATCCTCTGGAG	+8 +75	(4)
CDKN2A RT	CCAACGCACCGAATAGTTACG	CGCTGCCCATCATCATGAC		
CDKN2A SNaPshot (F+R)	TGGCTGGTCACCAGAGGGTG	GACCGTAACTATTCGGTGCG		(5)
CDKN2A SNaPshot	CCTCCTCTACCCGACCCC			
CDKN2A_MSP	TTATTAGAGGGTGGGGCGGATCGC	GACCCCGAACCGCGACCGTAA		(6)
CDKN2A_UMSP	TTATTAGAGGGTGGGGTGGATTGT	CAACCCCAAACCACAACCATAA		(6)
CRBP1 ChIP	CGTTTGAAGGAAATCCCCAG	GACGTTCAGTTCGTTTCCCC	-166 -265	
CDKN2A_Bis	AATAATGTGTAATTTTGTTTTTAGAATATTGAG	AAACTAAACTCCTCCCCACCTA	-120 -777	(7)
CRBP1 RT	TTGTGGCCAAACTGGCTCCA	ACACTGGAGCTTGTCTCCGT		(8)
CRBP1 RT-real time	CAGGCATAGATGACCGCAAGT	TGTCTCCGTCCCAGCTCACT		
α-Crystallin ChIP & RT	CCGTGGTACCAAAGCTGA	AGCCGGCTGGGGTAGAAG	+49 +133	(3)
GAPdH RT	ATCAAGAAGGTGGTGAAGCAG	CTTACTCCTTGGAGGCCATGT		
GATA4 ChIP	CCTGGACTTTGCCTGCTG	ACTGGCCTGTGGGAGTCAC	-55 -172	
HOXA9 ChIP	CTCAGGAGCCTCGTGTCTTT	GTGACCAGGTGGAGGTGTGT	+64 +145	
MLH1 ChIP	CACTGAGGTGATTGGCTGAA	GCCAGAAGAGCCAAGGAAAC	-10 +53	
MLH1 RT	AGCCTCTGAGCAAACCCCTGTC	CCATCTTCCTCTGTCCAGCCAC		
MLH1_RT real time	ACAGCTGATGGAAAGTGTGCAT	ATTGCCAGCACATGGTTTAGG		
MLH1 Bis	TTTTTTTAGGAGTGAAGGAGGTTA	CCCAAAAAAAACAAAATAAAAATC	-285 -559	
TIMP3 ChIP (CpG Island)	CTTTTTGGAGGGCCGATGA	CCCCCTCAGACCAATGGC	+765 +815	
TIMP3 ChIP (TSS)	AGTTTTGGATCAGCTCACCCC	ACAGAGCTCCACCCTTCAGC	-105 -155	
TIMP3 RT	GCTGTGCAACTTCGTGGAGAGG	CTCGGTACCAGCTGCAGTAGCC		(9)
TIMP3_RT real time	CTTCTGCAACTCCGACATCGT	AGCTTCTTCCCCACCACC TT		
TIMP3 Bis	TGGTTTGGGTTAGAGATATTTAGTG	AAACTCCAACTACCCAAAAACAC	+542 +1232	
MGMT ChIP	GCGCTTTCAGGACCACTC	GTGCCTTAGTTTGCCAAATG	-428 -329	
MGMT RT	ATGGACAAGGATTGTGAAATG	GAAAACGGGATGGTGAAGAGC		

References:

1. Csankovszki, G., Nagy, A. and Jaenisch, R. (2001) Synergism of Xist RNA, DNA methylation, and histone hypoacetylation in maintaining X chromosome inactivation. *J Cell Biol*, **153**, 773-784.
2. Hernandez-Munoz, I., Lund, A.H., van der Stoop, P., Boutsma, E., Muijrers, I., Verhoeven, E., Nusinow, D.A., Panning, B., Marahrens, Y. and van Lohuizen, M. (2005) Stable X chromosome inactivation involves the PRC1 Polycomb complex and requires histone MACROH2A1 and the CULLIN3/SPOP ubiquitin E3 ligase. *Proc Natl Acad Sci U S A*, **102**, 7635-7640.
3. Schlesinger, Y., Straussman, R., Keshet, I., Farkash, S., Hecht, M., Zimmerman, J., Eden, E., Yakhini, Z., Ben-Shushan, E., Reubinoff, B.E. *et al.* (2007) Polycomb-mediated methylation on Lys27 of histone H3 pre-marks genes for de novo methylation in cancer. *Nat Genet*, **39**, 232-236.
4. Egger, G., Aparicio, A.M., Escobar, S.G. and Jones, P.A. (2007) Inhibition of histone deacetylation does not block resilencing of p16 after 5-aza-2'-deoxycytidine treatment. *Cancer Res*, **67**, 346-353.
5. Bachman, K.E., Park, B.H., Rhee, I., Rajagopalan, H., Herman, J.G., Baylin, S.B., Kinzler, K.W. and Vogelstein, B. (2003) Histone modifications and silencing prior to DNA methylation of a tumor suppressor gene. *Cancer Cell*, **3**, 89-95.
6. Herman, J.G., Graff, J.R., Myohanen, S., Nelkin, B.D. and Baylin, S.B. (1996) Methylation-specific PCR: a novel PCR assay for methylation status of CpG islands. *Proc Natl Acad Sci U S A*, **93**, 9821-9826.
7. Gonzalgo, M.L., Hayashida, T., Bender, C.M., Pao, M.M., Tsai, Y.C., Gonzales, F.A., Nguyen, H.D., Nguyen, T.T. and Jones, P.A. (1998) The role of DNA methylation in expression of the p19/p16 locus in human bladder cancer cell lines. *Cancer Res*, **58**, 1245-1252.
8. Esteller, M., Guo, M., Moreno, V., Peinado, M.A., Capella, G., Galm, O., Baylin, S.B. and Herman, J.G. (2002) Hypermethylation-associated Inactivation of the Cellular Retinol-Binding-Protein 1 Gene in Human Cancer. *Cancer Res*, **62**, 5902-5905.
9. Rhee, I., Bachman, K.E., Park, B.H., Jair, K.W., Yen, R.W., Schuebel, K.E., Cui, H., Feinberg, A.P., Lengauer, C., Kinzler, K.W. *et al.* (2002) DNMT1 and DNMT3b cooperate to silence genes in human cancer cells. *Nature*, **416**, 552-556.